

Quantum Tomography of Inductively-Created Large Multiphoton States

E. Megidish,¹ A. Halevy,¹ Y. Pilnyak,¹ A. Slapak,² and H. S. Eisenberg¹

¹*Racah Institute of Physics, Hebrew University of Jerusalem, Jerusalem 9190401, Israel*

²*School of Electrical Engineering, Tel-Aviv University, Tel-Aviv 69978, Israel*

The generation of quantum entangled states of many particles is a central goal of quantum information science. Characterizing such states is a complex task that demands exponentially large resources as particles are being added. Previously, we demonstrated a resource efficient source that can generate, in principal, entanglement between any number of photons. This source recursively fuse photon pairs generated by a pulsed laser into a multiphoton entangled state. In the current work, we perform quantum state tomography on the photon pair source and quantum process tomography on the fusion operation. As a result, the full quantum Greenberger-Horne-Zeilinger (GHZ) state of any number of photons can be calculated. We explore the prospects of our scheme and calculate nonlocality and genuine N -photon entanglement thresholds for states with up to twelve photons.

PACS numbers: 03.67.Bg, 42.50.Dv, 42.50.Ex

Multiparticle entanglement between many quantum bits (qubits) is an important resource for quantum information science. It is required for quantum computation [1–3] and in quantum communication it enables error correction [4] and multiparty protocols, such as quantum secret sharing [5] and open destination teleportation [6]. Multiparticle entangled states have been shown to refute local realistic theories. The violation of these theories increases as the particle number is increased [7, 8]. These highly entangled states can also demonstrate non-local interference with a better resolution than that of the photons' fundamental wavelength, enhancing the optical measurement accuracy [9].

The process of parametric down-conversion (PDC) in nonlinear dielectric crystals is known to produce high-quality pairs of polarization entangled photons [10]. However, no efficient higher-order process exists that can directly create entanglement between more than two photons. One approach to create multiphoton entangled states is to split a high-order PDC event, in which more than one pump photon is down-converted [11, 12]. A different approach is to fuse photon pairs produced by PDC into a multiphoton quantum state. The largest state produced in this strategy to date is a ten-photon GHZ state [13]. Usually, the produced state is partially characterized and entanglement is verified by measurement of an entanglement witness operator [14].

Measuring the state of a quantum system is a task of high complexity, both experimentally and computationally. It requires many identical copies of the system which are projected onto different bases spanning the system's Hilbert space. The state's density matrix is then reconstructed from the different projection mea-

surement results, a procedure known as quantum state tomography (QST) [15]. If the quantum system is composed of n qubits, it is 2^n -dimensional, and the number of required projection measurements is 4^n . Even after sufficient amount of data about the state has been collected, the numerical process that is required to calculate the density matrix from the results scales as 16^n . The result of this scalability problem is that the largest state that has been fully characterized to date is a W-state of eight trapped ion qubits [16].

We have recently introduced a resource efficient setup that can create, in principle, entangled photon states of any number of photons [17]. A pump pulse is down-converted in a nonlinear crystal generating pairs of polarization entangled photons [10]. When a pair is generated, the photon in path a is directed to a polarization beam splitter (PBS, see Fig. 1), while the photon in path b enters a delay line. The delay time τ is chosen such that if a second entangled pair is generated by the next pump pulse, the photon of the second pair in path a meets the photon of the first pair in path b at the fusing PBS. Post-selecting the events in which one photon exits from each PBS output port (i.e., both photons have the same polarization), projects the two entangled pairs onto a four-photon GHZ state as follows

$$\begin{aligned} |\psi^+\rangle_{a,b}^{0,0} \otimes |\psi^+\rangle_{a,b}^{\tau,\tau} &\xrightarrow{\text{Delay}} |\psi^+\rangle_{a,b}^{0,\tau} \otimes |\psi^+\rangle_{a,b}^{\tau,2\tau} = \quad (1) \\ \frac{1}{2}(|h_a^0 v_b^\tau\rangle + |v_a^0 h_b^\tau\rangle) \otimes (|h_a^\tau v_b^{2\tau}\rangle + |v_a^\tau h_b^{2\tau}\rangle) &\xrightarrow{\text{PBS}} \\ \frac{1}{2}(|h_a^0 v_b^\tau v_a^\tau h_b^{2\tau}\rangle + |v_a^0 h_b^\tau h_a^\tau v_b^{2\tau}\rangle) &= |\text{GHZ}\rangle_{1,2,3,4}. \end{aligned}$$

h_x^t (v_x^t) is a horizontal (vertical) polarized photon traveling in path x at time delay t . According to this description, time only plays a role of an additional label to each

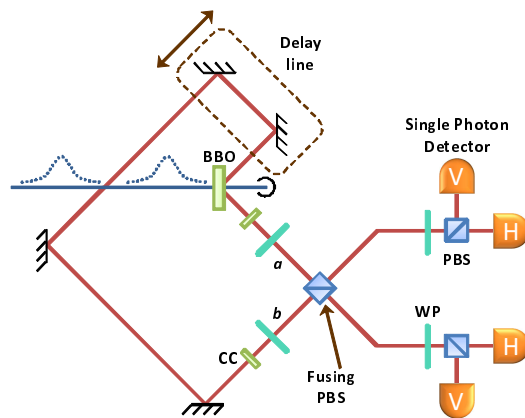


FIG. 1. (Color online) Experimental setup (see text for details).

of the photons 1, 2, 3, and 4. Theoretically, a third pair can be generated from the same source and its photon in path a will meet the delayed photon in path b of the second pair at the same fusing PBS. All the six photons from the three pairs will be projected onto a six-photon GHZ state. As long as additional consecutive pairs are generated, larger entangled states can be produced.

In this Letter, we show that due to the recursive nature of our scheme we are able to efficiently characterize the full density matrix of any measured GHZ state, and even larger states that could only be detected in principle after a very long wait. Such states, even if they are not actually being detected, do exist in the output amplitude of the setup with a very small probability amplitude. For this purpose, two building blocks of the scheme are fully characterized: the source photon pair state and the fusion quantum process, which are sufficient for calculating the full density matrix of any potentially-generated state. The simplicity of this procedure enables the measurement of the full density matrix of states of very high number of photons, which can not be characterized using standard QST otherwise.

The created GHZ states are fused together from a set of entangled photon pairs by several two-photon fusion operations. In the four-photon case the final quantum state is described by the following density matrix

$$\hat{\rho}_{1,2,3,4} = E(\hat{\rho}_{1,2} \otimes \hat{\rho}_{3,4})E^\dagger, \quad (2)$$

where $\hat{\rho}_{i,j}$ is the photon pair density matrix of the i^{th} and the j^{th} photons, and E is the operator describing the four-photon entangling process. Only photons 2 and 3 (at time τ) are "interacting" at the PBS. Therefore, E can be written as

$$E = \sigma_0^1 F_{2,3} \sigma_0^4, \quad (3)$$

$F_{2,3} = (|h_2 h_3\rangle\langle h_2 h_3| + |v_2 v_3\rangle\langle v_2 v_3|) = \frac{1}{2}(\sigma_0^2 \sigma_3^3 + \sigma_3^2 \sigma_3^3)$, where σ_0^i and σ_3^i are the identity and Pauli z matrices when applied to the i^{th} photon. In our scheme all the

pairs originate from the same source, and consequently they are described by the same density matrix. In addition, the fusion operation is also identical, as photons from consecutive pairs meet at the same PBS. Thus, by measuring the two matrices $\hat{\rho}_{1,2}$ and $F_{2,3}$, the density matrix of any potentially-generated GHZ state can be calculated by combining identical two-photon states with identical projections

$$\begin{aligned} \hat{\rho}_{1,2,\dots,n} &= \sigma_0^1 F_{2,3} \cdots F_{n-2,n-1} \sigma_0^n \\ &(\hat{\rho}_{1,2} \otimes \cdots \otimes \hat{\rho}_{n-1,n}) \\ &(\sigma_0^1 F_{2,3} \cdots F_{n-2,n-1} \sigma_0^n)^\dagger. \end{aligned} \quad (4)$$

The entire information about a GHZ state containing any number of photons is achievable, without accumulating their full statistics or even observing them.

Polarization entangled photon pairs are created by the non-collinear type-II PDC process [10]. A pulsed Ti:Sapphire laser source with a 76 MHz repetition rate is frequency doubled to a wavelength of 390 nm with an average power of 400 mW. The laser beam is corrected for astigmatism and focused on a 2 mm thick β -BaB₂O₄ (BBO) crystal (see Fig. 1). Compensating crystals (CC) correct for temporal walk-offs. In addition, tilting of the compensating crystal in path a is used to control the phase φ of the state

$$|\psi(\varphi)\rangle_{a,b}^{0,0} = \frac{1}{\sqrt{2}}(|h_a^0 v_b^0\rangle + e^{i\varphi}|v_a^0 h_b^0\rangle), \quad (5)$$

e.g., for $\varphi = 0$ the resulting state is the maximally entangled Bell state $|\psi^+\rangle$. Half-wave plates (HWP) and quarter-wave plates (QWP) are used to analyze the photons in a rotated basis. The 780 nm wavelength down-converted photons are spatially filtered by coupling them into and out of single-mode fibers, and spectrally filtered by using 3 nm wide bandpass filters. The pair generation rate is 40,000 per second, and the four-photon rate is 8.5 per second.

One photon from the first pair is delayed until another pump pulse arrives at the generating crystal by a 31.6 m long (105 ns) free-space delay line. The delay time enables the fusion of pairs which are separated by eight consecutive laser pulse. This delay time is also longer than the dead time of the single photon detectors (50 ns, Perkin Elmer SPCM-AQ4C). The delay line is built from highly reflective dielectric mirrors, with an overall transmittance higher than 90% after 10 reflections. Less than 10% of the signal is sampled into a single mode fiber as a feedback signal that is used to stabilize the delayed beam's spatial properties, by tilting a piezo-mounted mirror in the middle of the delay line. Before any scan the delay time is measured and calibrated using two-photon interference measurements.

First, we performed standard QST and reconstructed the pair density matrix $\hat{\rho}_{1,2}$ [15]. When we consider detection of only pairs, the fusing PBS serves as the polarization analyzer (see Fig. 1). The polarization basis is

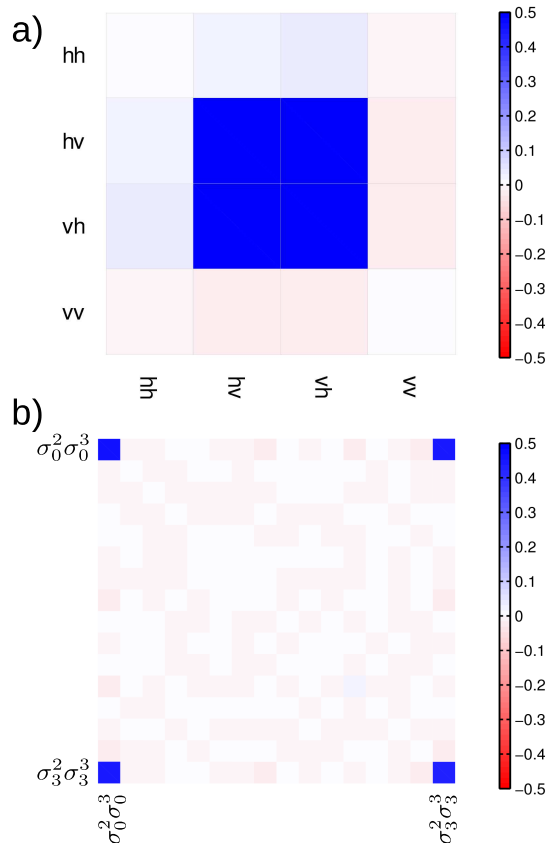


FIG. 2. a) Real part of the photon pair density matrix, $\hat{\rho}_{1,2}$. The polarization entangled pairs are generated with a 97.7% overlap with the $|\psi^+\rangle$ Bell state. b) Real part of the χ matrix representing the fusion operation measured by AAPT technique.

controlled using wave plates in each path (*a* and *b*) prior to the fusing PBS. We discriminate between the photons by their arrival times to the detectors (0 and τ). As a result, each photon polarization amplitude is labelled in time and space (0 and τ , a and b). The two photon state, as can be seen in Fig. 2(a), was measured to have a 97.7% overlap with the $|\psi^+\rangle$ state.

Next, we measured the fusing operation between photons 2 and 3. In a standard quantum process tomography one should measure the process output for different input states [19]. We used ancilla-assisted process tomography (AAPT) [18], where each input photon is entangled to another photon and a QST is performed to all four photons. In AAPT, the input polarization states of the quantum process are controlled by measuring the ancillary entangled photons in different polarization bases. This is also manifested by the Choi-Jamiołkowski isomorphism between completely positive maps and quantum states [20].

In our case, the fusion process of photons 2 and 3 can be extracted from the initial pair density matrix, $\hat{\rho}_{1,2}$, and by performing QST on the final four-photon state.

Four-photon QST requires at least 256 different projections to span the entire four-photon polarization Hilbert space. For the polarization manipulation of the two photons at time τ we used WPs positioned after the fusing PBS. The polarization states of photons 1 and 4 arriving at times 0 and 2τ are controlled non-locally by the WPs and the birefringent phase φ before the fusing PBS (see supplemental material of Ref. [21] for more details). The 256 probabilities were measured by the four detectors using 81 WPs configuration. Each configuration was integrated for 30 seconds and after each set the delay line was calibrated. We repeated this sequence 78 times.

The process operator can be represented in the Pauli basis as

$$\hat{\rho}_{1,2,3,4} = \sum_{i,j=0}^3 \chi_{i,j} (\sigma_0^1 \sigma_i^2 \sigma_j^3 \sigma_0^4) (\hat{\rho}_{1,2} \otimes \hat{\rho}_{3,4}) (\sigma_0^1 \sigma_i^2 \sigma_j^3 \sigma_0^4)^\dagger, \quad (6)$$

where $\chi_{i,j}$ is the process coefficient matrix which completely and uniquely describes the process. The χ matrix is reconstructed from the measured initial state $\hat{\rho}_{1,2}$ and the projection measurements of the final state $\hat{\rho}_{1,2,3,4}$, by a maximal likelihood fit to Eq 6 (see Fig. 2(b)). We then calculated the four-photon density matrix using the fusion operation and the pair density matrix (see Fig. 3(a)). Two distinct populations ($h_1 v_2 v_3 h_4$ and $v_1 h_2 h_3 v_4$) with the corresponding coherence terms are clearly observed, in accordance with the expected four-photon GHZ state of Eq .1. The fidelity between the calculated four-photon GHZ state and the ideal one is $(85.4 \pm 0.2)\%$. Furthermore, we calculated the six-photon density matrix (see Fig. 3(b)). Similar to four-photon state the six-photon state also shows the GHZ characteristics with fidelity $(74.3 \pm 0.4)\%$. Experimentally we detected six-photons events at a rate of 20 events per hour.

Errors were estimated with a bootstrap method, by a Monte Carlo simulation of the fusion reconstruction process. Due to the high flux of pairs (40,000 per second) the errors in the pair density matrix were neglected. Each projection measurement of the final state $\hat{\rho}_{1,2,3,4}$ is assumed to have a Poissonian error distribution around the average event count. Numerically, we created 100 randomly distributed measurement samples. For each sample, the χ process matrix was reconstructed by the maximal likelihood procedure. We calculated the difference measures for the entire error sample $\{\chi\}_1^{100}$ and took the standard deviation as the error.

The four-photon fidelity is mainly affected by distinguishability between photons 2 and 3. The photons can be distinguished (labelled) by their arrival time, spectrum, angle, beam width, and position. The setup was optically designed, calibrated and actively stabilized to minimize these distinguishabilities. Nevertheless, minute

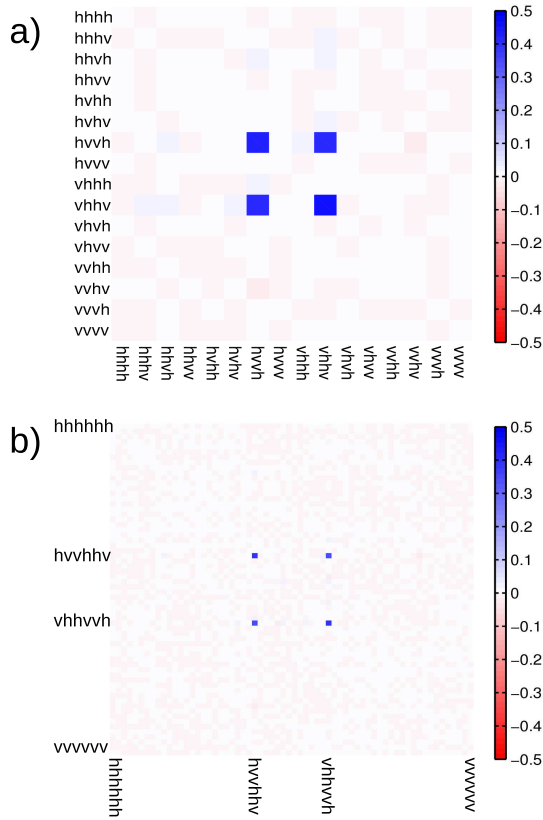


FIG. 3. (Color online) Real part of the four-photon , (a) and six-photon density matrices (b). The states were calculated from the fusion process and the photon pair density state.

temperature changes and spectral difference between the photons due to the PDC process [23] introduce some distinguishability. In addition, the polarization of photons 1 and 4 is controlled by nonlocal rotations. Though the pair fidelity is high (97.7%), some polarization rotation error is unavoidable and therefore some inaccuracy is introduced to the AAPT.

Using the fully characterized two-photon density matrix and the fusion process matrix, we calculated the full density matrices of six, eight, ten, and twelve photons, and their fidelities with the corresponding GHZ states (see Fig. 4). As more pairs are added, the overlap between the N -photon GHZ state and the calculated state decreases due to the imperfect fusion operation. Genuine N -photon entanglement for GHZ states requires fidelity above 50% [22]. We currently satisfy this condition up to ten photons, where the value for twelve photons is $(49.3 \pm 0.65)\%$.

Multiphoton entangled states with higher photon numbers refute local realism with increasing violation. Bell inequalities for N -particle GHZ state with different num-

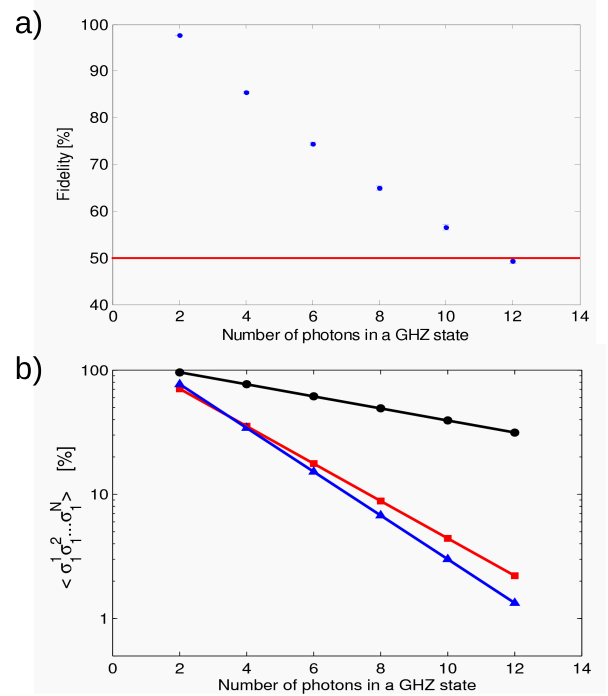


FIG. 4. (a) Fidelity between an ideal N -photon GHZ state and the state calculated from the pair density matrix and the fusion operation as a function of the number of photons. Red line indicates the 50% fidelity threshold required for genuine N -photon entanglement. Errors were calculated as described in the main text. (b) (black) Calculated interference visibility when all photons are rotated to the p/m basis as a function of the number of photons in the GHZ state. Threshold visibility required to violate local realism according to Żukowski *et al.* (red) [8] and Mermin (blue) [7].

ber of measurement settings set a criteria for the threshold visibility for refuting local realistic theories [7, 8]. We have calculated the expectation value of the $\sigma_1^1 \sigma_1^2 \dots \sigma_1^N$ operator corresponding to the visibility when the photons are measured in the $p/m = h \pm v$ basis, and compared them to the threshold values obtained by Mermin [7] and Żukowski *et al.* [8] (see Fig. 4). The computed visibility for any possibly generated GHZ state from our setup refute local realism according to the criteria above (see Fig. 4).

In conclusion, we have measured the pairs' density matrix and the fusion operation of our multiphoton entanglement setup. The full quantum state of any potentially-generated GHZ state can be calculated without even detecting the relevant photons, avoiding the experimental and computational complexity that is usually required for the characterization of such states. For the first time, we can experimentally explore the different prospects of schemes that generate multiphoton entanglement with high photon numbers. Currently, our system has the po-

tential of refuting local realistic theories in any number of photons and to generate genuine multiphoton entangled states of up to ten photons.

The authors thank the Israeli Science Foundation for supporting this work under grants 546/10 and 793/13.

-
- [1] R. Raussendorf and H.-J. Briegel, *Phys. Rev. Lett.* **86**, 5188 (2001).
- [2] P. Walther, K.J. Resch, T. Rudolph, E. Schenck, H. Weinfurter, V. Vedral, M. Aspelmeyer, and A. Zeilinger, *Nature* **434**, 169 (2005).
- [3] D. Deutsch, *Proc. R. Soc. London Ser. A* **400**, 97 (1985).
- [4] D. Schlingemann and R.F. Werner, *Phys. Rev. A* **65**, 012308 (2002).
- [5] M. Hillery, V. Bužek, and A. Berthiaume, *Phys. Rev. A* **59**, 1829 (1999).
- [6] Z. Zhao, Y.-A. Chen, A.-N. Zhang, T. Yang, H.J. Briegel, and J.-W. Pan, *Nature* **430**, 19 (2004).
- [7] N. D. Mermin, *Phys. Rev. Lett.* **65**, 1838 (1990).
- [8] M. Żukowski and D. Kaszlikowski, *Phys. Rev. A* **56**, R1682 (1997).
- [9] P. Walther, J.-W. Pan, M. Aspelmeyer, R. Ursin, S. Gasparoni, and Anton Zeilinger, *Nature* **429**, 158 (2004).
- [10] P.G. Kwiat, K. Mattle, H. Weinfurter, A. Zeilinger, A. V. Sergienko, and Y.H. Shih, *Phys. Rev. Lett.* **75**, 4337 (1995).
- [11] A. Halevy, E. Megidish, T. Shacham, L. Dovrat, and H. S. Eisenberg, *Phys. Rev. Lett.* **106**, 130502 (2011).
- [12] N. Kiesel, C. Schmid, G. Tóth, E. Solano, and H. Weinfurter, *Phys. Rev. Lett.* **98**, 063604 (2007).
- [13] X.-L. Wang *et al.*, *Phys. Rev. Lett.* **117**, 210502 (2016).
- [14] O. Gühne, C.-Y. Lu, W.-B. Gao, and J.-W. Pan, *Phys. Rev. A* **76**, 030305(R) (2007).
- [15] D.F.V. James, P.G. Kwiat, W.J. Munro, and A.G. White, *Phys. Rev. A* **64**, 052312 (2001).
- [16] H. Häffner, W. Hänsel, C. F. Roos, J. Benhelm, D. Chekhalkar, M. Chwalla, T. Körber, U. D. Rapol, M. Riebe, P. O. Schmidt, C. Becher, O. Gühne, W. Dür, and R. Blatt, *Nature* **438**, 643 (2005).
- [17] E. Megidish, T. Shacham, A. Halevy, L. Dovrat, and H. S. Eisenberg, *Phys. Rev. Lett.* **109**, 080504 (2012).
- [18] M. Mohseni, A.T. Rezakhani, and D.A. Lidar, *Phys. Rev. A* **77**, 032322 (2008).
- [19] J.L. O'Brien, G.J. Pryde, A. Gilchrist, D. F. V. James, N. K. Langford, T.C. Ralph, and A.G. White, *Phys. Rev. Lett.* **93**, 080502 (2004).
- [20] A. Jamiolkowski, *Rep. Math. Phys.* **3**, 275 (1972).
- [21] E. Megidish, A. Halevy, T. Shacham, T. Dvir, L. Dovrat, and H. S. Eisenberg, *Phys. Rev. Lett.* **110**, 210403 (2013).
- [22] C. A. Sackett, D. Kielpinski, B. E. King, C. Langer, V. Meyer, C. J. Myatt, M. Rowe, Q. A. Turchette, W. M. Itano, D. J. Wineland, and C. Monroe, *Nature* **404**, 256 (2000).
- [23] P. J. Mosley, J. S. Lundeen, B. J. Smith, P. Wasylczyk, A. B. U'Ren, C. Silberhorn, and I. A. Walmsley, *Phys. Rev. Lett.* **100**, 133601 (2008).